

Fabrication of CdS/Ag/LPTNSs heterojunctions for visible light driven photocatalytic degradation of organic pollutant

Y. X. Jin^{a,†}, T. T. Guo^{c,†}, M. H. Wang^d, J. Tan^c, H. X. Ma^c, Y. Lian^{b,*}

^a*Jiaying Huanke Environmental New Material Technology Co., LTD, Jiaying 314001, China*

^b*College of Material and Textile Engineering, Jiaying University, Jiaying 314001, China*

^c*College of Biological, Chemical Sciences and Engineering, Jiaying University, Jiaying 314001, China*

^d*Jiaying Haiyan Ecological Environment Monitoring Station, Jiaying 314300, China*

Ternary CdS/Ag/LPTNSs heterojunctions were prepared by a two-step method. The prepared photocatalysts were characterized by transmission electron microscopy (TEM), X-ray photoelectron spectroscopy (XPS), X-ray diffraction (XRD), specific surface area analyzer (BET), photoluminescence (PL) spectroscopy and photoelectrochemical (PEC) measurement. The results showed that the prepared LPTNSs had lamellar multilayer structure and uniformly distributed silver particles and CdS on their surface. The PEC and PL results show that the formation of ternary heterojunction structure can improve the efficiency of photogenerated electron and hole separation. Under visible light irradiation, the photodegradation of methylene blue (MB) in the presence of various photocatalysts showed that photocatalytic performance of CdS/Ag/LPTNSs was better than that of P25, LPTNSs, CdS, Ag/LPTNSs and CdS/LPTNSs. A maximum removal efficiency of MB reached 84% within 90 min over CdS/Ag/LPTNSs. Moreover, the kinetic constant of CdS/Ag/LPTNSs is 11.8, 10.4, 4.3, 2.4 and 1.7 times as much as that of P25, LPTNSs, CdS, Ag/LPTNSs and CdS/LPTNSs, respectively. In addition, the repeated photodegradation study showed that CdS/Ag/LPTNSs exhibited good stability, and the removal rate still reached 83% after 4 cycles. This work provides a simple and low-cost method for the synthesis of ternary CdS/Ag/LPTNSs nanocomposite to photocatalytic degradation of organic pollution.

(Received March 26, 2022; Accepted July 23, 2022)

Keywords: Titanic acid, Solvothermal, Heterojunction, Photocatalytic degradation

* Corresponding author: hnlianyuan@126.com

† These authors contributed equally to this work

<https://doi.org/10.15251/DJNB.2022.173.811>

1. Introduction

With the rapid development of technology and industry, especially the paper and dye production, more industrial wastewater with toxicity has caused great pollution and serious damage to the ecological environment^[1-3]. Therefore, advanced technology to treat dye-containing wastewater is highly desired^[4,5]. Photocatalytic degradation technology based on semiconductors has attracted much attention due to its high efficiency and low-cost^[6]. There is much effort in the development of high-efficiency photocatalysts for degradation of organic dyes^[7-9].

Two-dimensional titania nanosheets (TNSs) have attracted wide attention in photocatalytic applications due to its low cost, large surface, thin thickness, low toxicity, and high chemical stability^[10]. However, their large bandgap can only allow optical response to UV light, together with rapid recombination of photogenerated electron-hole pairs, which restricts practical applications. To overcome these problems, pristine TNS has been modified by various methods, such as nanostructure design, metal/nonmetal element doping, surface modification, and heterojunction construction^[11]. Among them, heterojunction construction with narrow bandgap semiconductors is considered as the most effective way.

CdS with the bandgap of 2.42 eV is an ideal candidate for the heterojunction formation of CdS/TNS, owing to more negative CB of CdS than that of TNS^[12]. Kameyama *et al.* reported the synthesis of inorganic semiconductor multilayer thin films of CdS nanoparticles with TNS by electrostatic layer-by-layer accumulation^[13]. Tian *et al.* encapsulated CdS nanoparticles into TNS via an exfoliation-restacking method^[14]. Vijayan *et al.* reported an in-situ synthesis of TNS-CdS nanoparticle composite with excellent photocatalytic activity^[15]. Even though CdS/TNS composite photocatalysts prepared via different synthetic routes exhibit enhanced photocatalytic activities, instability is still a major issue. To improve the stability of CdS/TNS, one of the effective methods is to load cocatalyst to further improve the separation of electron-hole pairs. Ag is very stable and highly resistant to oxidation^[16]. Therefore, loading Ag nanoparticles (NPs) on the surface of TNS covered by CdS may be a useful way to improve its stability as well as the separation of carriers.

In this work, we report a ternary CdS/Ag/LPTNSs heterojunction composed of CdS NPs and Ag-loaded titanic acid with lamellar multilayer structure (LPTNSs), which is fabricated by a simple one-pot hydrothermal method and in-situ decomposition process. The samples were characterized by transmission electron microscopy (TEM), X-ray photoelectron spectroscopy (XPS), X-ray diffraction (XRD), photoluminescence (PL) spectroscopy and photoelectrochemical (PEC) measurement. The as-prepared photocatalysts were evaluated in the methylene blue (MB) degradation under visible light irradiation and exhibited excellent photocatalytic activity while compared with pure TNS photocatalyst. This can be attributed to Ag/LPTNSs as an excellent substrate for improving the dispersion of CdS and the interfacial contact among composites facilitating the transfer of photogenerated electrons during the photocatalysis.

2. Experiment

The commercial chemicals were used as received without further purification. Deionized water was obtained from local sources.

2.1. Synthesis of CdS/Ag/LPTNSs

2.1.1. Synthesis of Ag/LPTNSs

0.10 g AgNO₃ was dispersed in 60.0 mL NH₃·H₂O (14% wt) and stirred vigorously for 30 min. Then 5.0 mL tetrabutyl titanate and 2.0 mL isopropanol were slowly added dropwise to the above solution, followed by stirring for another 30 min. After that, the solution was then poured into a Teflon-lined autoclave and heated to 130 °C for 12 h. The autoclave was then cooled to room temperature. Subsequently, the white precipitate obtained was filtered and washed several times with deionized water until pH=7, then dried at 70 °C for 12 h to obtain Ag/TNSs nanocomposite. For comparison, TNSs were prepared by the same method.

2.1.2 Synthesis of CdS/Ag/LPTNSs

The above Ag/TNSs nanocomposite was dispersed in 100 mL deionized water and stirred for 1 h. Then 15.0 mL of 0.10 mol/L Cd(NO₃)₂ solution was added and stirred for another 2 h in a constant temperature water bath at 40 °C. After stirring, 15.0 mL of 0.10 mol/L Na₂S solution was added and stirred for 12 h. After that, the products were subsequently filtered, washed with deionized water and absolute ethanol, dried and collected. The obtained samples were denoted as CdS/Ag/TNSs. For comparison, CdS/TNSs was also prepared by the similar way.

2.2. Characterization

The microstructures of the as-synthesized samples were studied by JEOL JEM 2100 transmission electron microscope (TEM) at an accelerating voltage of 200 kV. The phase of the as-prepared samples was determined by Bruker D8 X-ray diffractometer (XRD) with graphite monochromatized Cu K α radiation. X-ray photoelectron spectroscopy (XPS) measurements were operated on a Thermo Scientific ESCA Lab 250 instrument with Al K α X-ray as the exciting source. The UV-vis spectra were carried out using a UV-vis spectrophotometer (UV-2550). The Brunauer-Emmett-Teller (BET) surface area were measured using the ASAP2020 physisorption Analyzer. The photoluminescent (PL) spectra were recorded on a HORIBA FluoroMax+. ESR testing were carried out using BRUKER A300.

2.3. Photoelectrochemical (PEC) measurements

The photoelectrochemical analysis were tested on a CHI 660E electrochemical workstation (Shanghai Chenhua Instrument Co., Ltd, China) in a three-electrode system with a Pt wire as the counter electrode and saturated calomel as the reference electrode. The working electrode was prepared by spinning the suspension (50 mg of photocatalyst dispersed in 10 mL of absolute alcohol) onto a cleaned FTO glass surface with an area of 1×2 cm². 1 M Na₂SO₄ aqueous solution were employed as the electrolyte. A 300 W Xe lamp was used as the light source with a cutoff filter ($\lambda \geq 400$ nm).

2.4. Photocatalytic performance

2.4.1. MB removal experiment

The photocatalytic activity of prepared photocatalysts were investigated by methylene blue (MB) degradation. Typically, 30 mg photocatalyst of CdS/Ag/TNSs was suspended in 100 mL MB solution (10, 20, 30 and 40 mg/L) taken in a beaker and kept in the dark chamber for 1 h with continuous stirring in order to obtain adsorption-desorption equilibrium. The initial absorbance of

the solution was measured by UV-vis spectrophotometer. The solution was irradiated under continuous stirring by using a mercury lamp as light source with attached UV filters. About 2.0 ml of MB solution were drawn from the photoreactor at 10 min intervals and centrifuged at 10000 rpm for 3 min to isolate the photocatalyst. The absorbance of each supernatant solution was recorded at characteristic MB peak (662 nm) and continued for 90 min. The rate constant of methylene blue degradation in presence of each sample was calculated as the slope of $-\ln(C/C_0)$ versus time plots.

2.4.2. Reusability test

A fixed amount of CdS/Ag/LPTNSs (30 mg) was dispersed in 100.0 mL of MB solution (10.0 mg/L) and stirred for 1 h. After the first cycle, MB solutions were centrifuged at 10000 rpm and the photocatalyst CdS/Ag/LPTNSs was recycled by centrifugation and then dried in an oven for 12 h. Then the sample was directly applied to the next recycle and this process was repeated for 4 cycles. Supernatant was collected from every recycle and residual dye concentrations were measured.

3. Results and Analysis

3.1. Structure and morphology

Figs. 1(a-b) shows the TEM image of as-prepared CdS/Ag/LPTNSs nanocomposite. For the CdS/Ag/LPTNSs nanocomposite, the sheet-like morphology is observed. Additionally, it can also be observed that several small nanoparticles are embedded in the nanosheets. The interlayer spacing of 0.77 nm for TNSs with multilayer structures is displayed in Fig. 1(c), which is consistent with previous research^[17]. In Fig. 1(d), the lattice fringes about 0.33 nm and 0.224 nm are ascribed to the plane of anatase CdS (111) and Ag (111), respectively^[18]. The result indicated that the Ag and CdS NPs were loaded on the surface of LPTNSs with tight contact and formation of heterostructure at the interfaces.

The XRD patterns of P25 and LPTNSs are shown in Fig. 2. In Fig. 2(a), the 2θ values of LPTNSs are located at 10.5° , 28.0° , 48.0° , 63° , which matches with $H_2Ti_3O_7$ with lower crystallinity, corresponding to (200), (310), (020) and (202) planes, respectively^[15]. The commercial P25 is displayed mainly in crystallized anatase TiO_2 (JCPDS No. 21-1272). In Fig. 2(b), the typical peaks at 26.5° , 43.9° and 52.1° are observed for CdS/LPTNSs and CdS/Ag/LPTNSs, which is resulted from the (111), (220) and (311) planes of cubic CdS (JCPDS No. 75-0581)^[15]. XRD analysis proved that LPTNSs and CdS were combined successfully. However, compared LPTNSs with Ag/LPTNSs, no obvious characteristic peaks for Ag are observed and the two XRD patterns were almost similar, which may be ascribed to the low content of Ag NPs on the surface of LPTNSs.

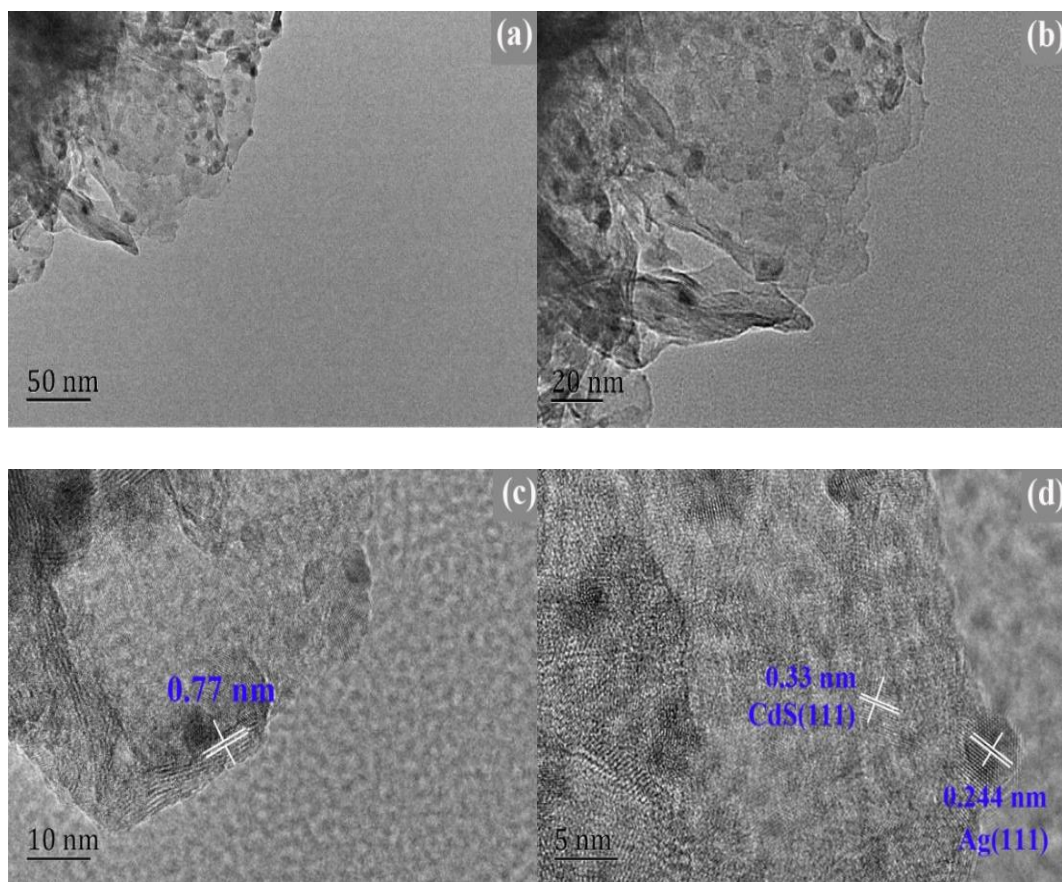


Fig. 1. TEM images of CdS/Ag/LPTNSs (a-b); HRTEM images of CdS/Ag/LPTNSs (c-d).

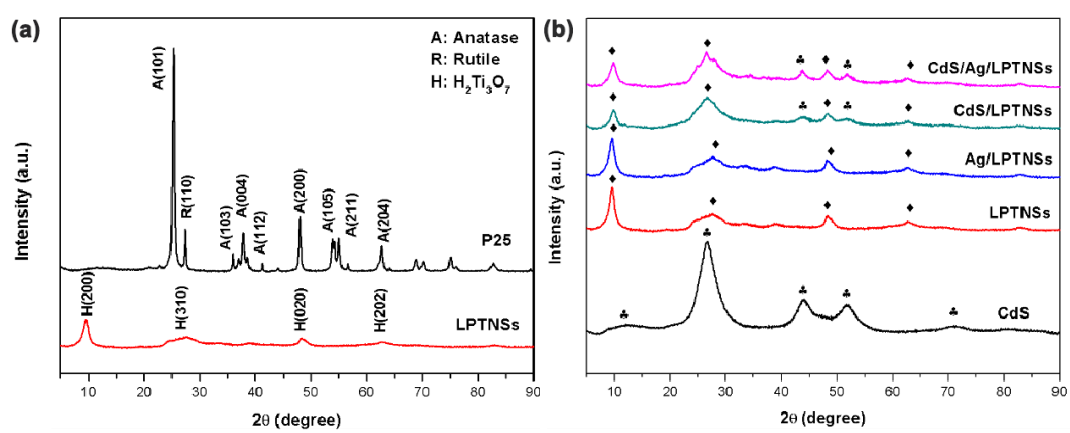


Fig. 2. XRD patterns of as-prepared samples.

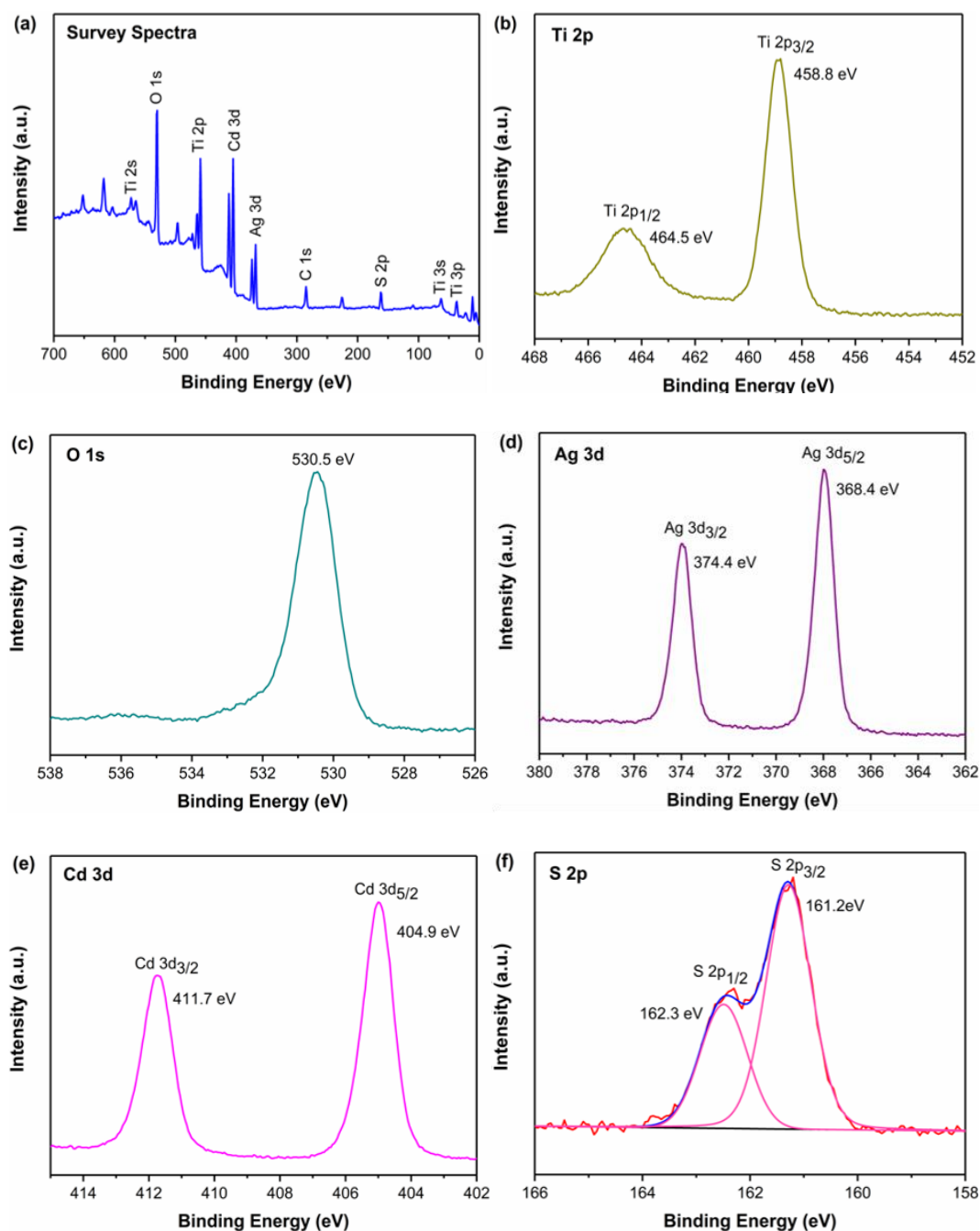


Fig. 3. XPS full spectrum of CdS/Ag/LPTNSs (a) and fine energy spectrum of each element (b-f).

XPS analysis was also performed to determine the surface element composition and chemical state of CdS/Ag/LPTNSs and results are presented in Fig. 3. As shown in Fig. 3(a), the ternary CdS/Ag/LPTNSs was composed of Cd, S, O, Ti and Ag elements. Fig. 3(b) shows Ti 2p spectrum with binding energy at 458.8 eV and 464.5 eV, which is ascribed to Ti 2p_{3/2} and Ti 2p_{1/2}, suggesting the existence of the Ti⁴⁺ oxidation state^[19]. Fig. 3(c) displays O 1s spectrum and its binding energies are located at 530.5 eV related to Ti-O^[20]. Fig. 3(d) gives Ag 3d spectrum with binding energy at 368.4 and 374.4 eV, which are assigned to Ag 3d_{5/2} and Ag 3d_{3/2}, which hinted

that silver was metallic nature ^[21]. Fig. 3(e) shows Cd 3d spectrum with binding energy at 404.9 and 411.7 eV, which is related to Cd 3d_{5/2} and Cd 3d_{3/2}, respectively ^[22]. The S 2p spectrum in Fig. 3(f) shows binding energy at 161.2 and 162.3 eV, which is assigned to S 2p_{3/2} and S 2p_{1/2}, suggesting that element sulfur was presented as S²⁻ ^[18].

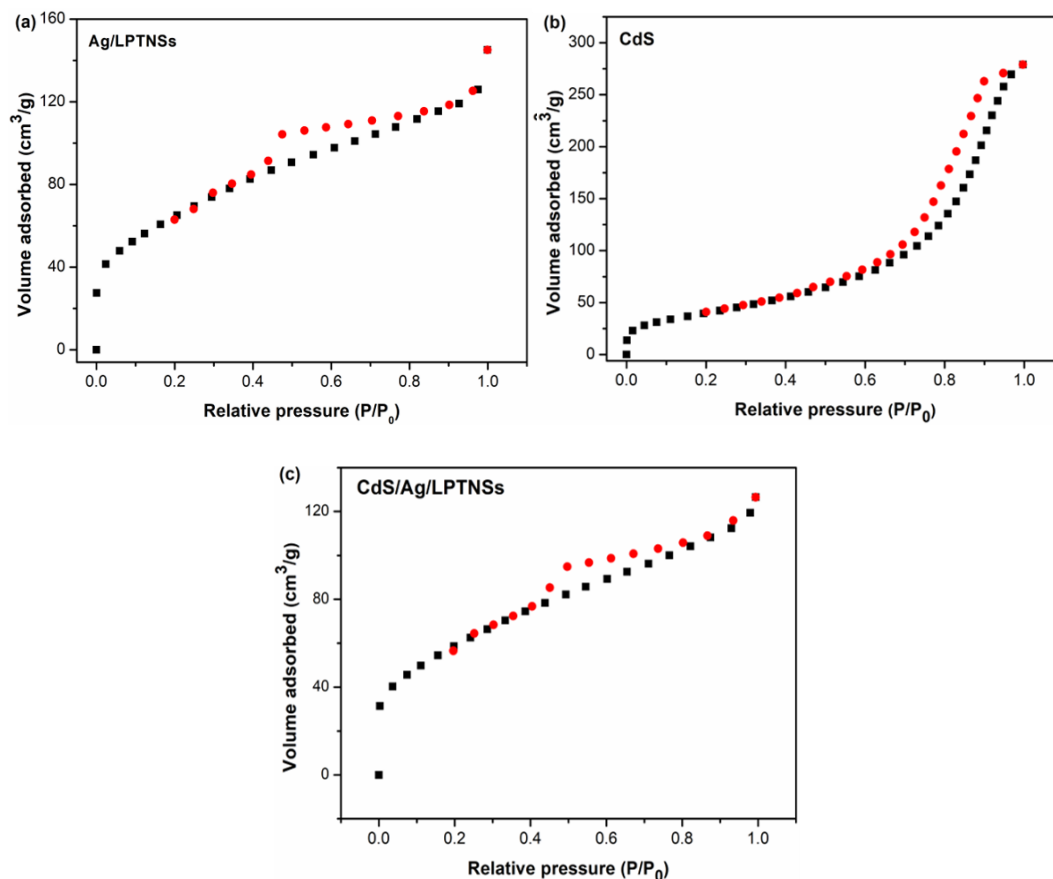


Fig. 4. N₂ adsorption-desorption isotherms curves of (a) Ag/LPTNSs, (b) CdS and (c) CdS/Ag/LPTNSs.

Fig. 4 showed the N₂ sorption isotherms curves of Ag/LPTNSs, CdS and CdS/Ag/LPTNSs. The Ag/LPTNSs, CdS and CdS/Ag/LPTNSs showed type IV isotherm with H3 hysteresis loop, which displayed mesoporous structures in the samples ^[23]. Additionally, the specific surface areas of Ag/LPTNSs, CdS and CdS/Ag/LPTNSs are 235.243, 148.287 and 214.348 m²/g, and the pore sizes are 3.817, 3.563, 3.651 nm (Table 1). The specific surface areas and pore size of CdS/Ag/LPTNSs is smaller than Ag/LPTNSs, which could be attributed to the anchoring of CdS on the layered surface. Moreover, compared with CdS nanoparticles, CdS/Ag/LPTNSs has the higher specific surface area, which will not only provide more active sites facilitating the progress of photocatalytic reactions, but also alleviate the accumulation of CdS nanoparticles ^[24,25].

Table 1. The specific surface areas and pore size of different samples.

Sample	BET surface area ($\text{m}^2 \cdot \text{g}^{-1}$)	Pore diameter (nm)
Ag/LPTNSs	235.243	3.817
CdS	148.287	3.563
CdS/Ag/LPTNSs	214.348	3.651

3.2. Photoelectrochemical (PEC) and PL properties

To further evaluate the charge separation efficiency of the samples, transient photocurrent response measurements were carried out with shown in Fig. 5(a). The photocurrent intensity of Cd/Ag/LPTNSs is higher than that of LPTNSs, Ag/LPTNSs, CdS, CdS/LPTNSs and P25, indicating the higher separation and transfer rate of photoinduced charge carriers in Cd/Ag/LPTNSs. In addition, in the EIS Nyquist plots (Fig. 5(b)), the smallest arc radius is observed in Cd/Ag/LPTNSs, suggesting superior electronic conductivity and better charge transfer efficiency^[26].

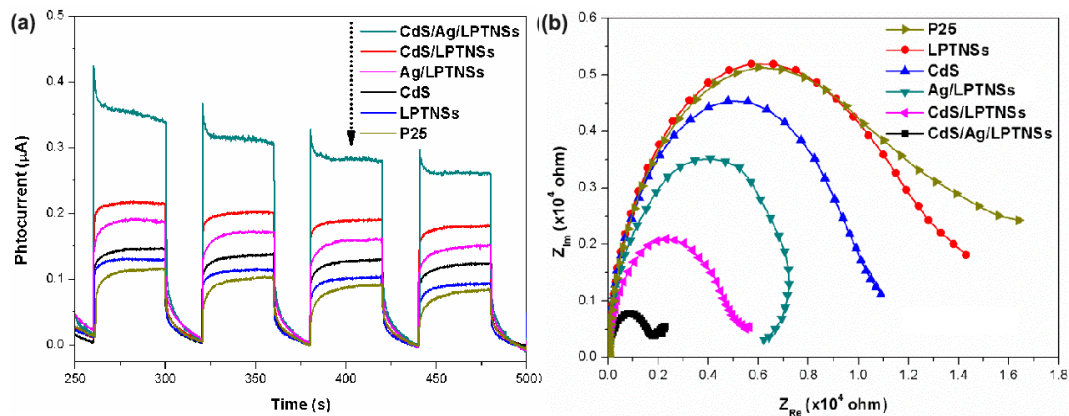


Fig. 5. (a) Transient photocurrent response and (b) EIS Nyquist plots of different samples.

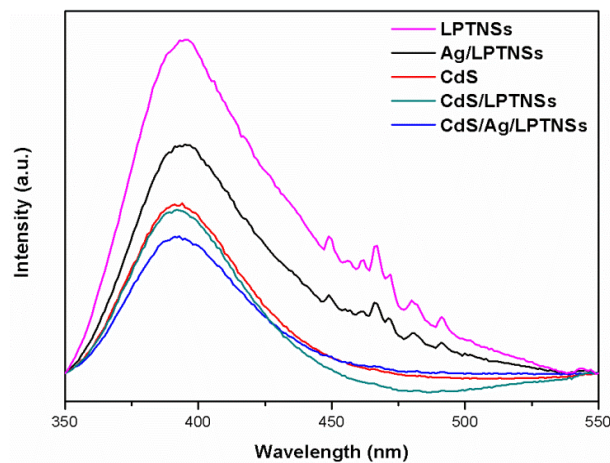


Fig. 6. PL spectra of the as-obtained samples.

PL measurements were also performed at room temperature to help understand the separation efficiency of photogenerated charge carriers, and the results are shown in Fig. 6. The Cd/Ag/LPTNSs shows a weaker PL emission intensity than LPTNSs, Ag/LPTNSs, CdS, and CdS/LPTNSs, implying the formed ternary heterostructure has significantly improved the photogenerated charge separation efficiency.

3.3. Photocatalytic performance and reactive species determination

MB dye solution was used as the target pollutant to evaluate the photocatalytic performance of the prepared samples. As shown in Fig. 7(a), the absorption of MB varies for different samples. After 90 min irradiation, the degradation rates of MB were as follows: 12% for P25, 14% for LPTNSs, 32% for CdS, 50% for Ag/LPTNSs, 65% for CdS/LPTNSs and 84% for CdS/Ag/LPTNSs. The optimized photocatalytic activity of CdS/Ag/LPTNSs was 7 or 6 times larger than that of P25 or LPTNSs. For a better comparison of the photocatalytic activity of as-prepared samples, the kinetic model for degradation of MB aqueous solution was discussed as shown in Fig. 7(b). It was generally received that kinetics for photocatalysis can be described in terms of Langmuir-Hinshelwood (L-H) model, which can be expressed by following equation when the initial concentration of dye was relatively lower.

$$-\ln(C/C_0) = kt$$

where C_0 is the initial concentration of MB, C is the current concentration of MB, and k is the first-order rate constant, which can be used as assessment index for evaluating the photocatalytic efficiency of different samples. Fig. 7(b) shows that the plot of $-\ln(C/C_0)$ and irradiation time (t) is approximate linear. In Fig. 6(b), the reaction rate constants are determined as 0.0015, 0.0017, 0.0041, 0.0073, 0.0103 and 0.0177 min^{-1} for P25, LPTNSs, CdS, Ag/LPTNSs, CdS/LPTNSs and CdS/Ag/LPTNSs, respectively. The reaction constants k of MB photodegradation for CdS/Ag/LPTNSs were highest among the samples.

Fig. 7(c) shows the photocatalytic behavior of CdS/Ag/LPTNSs for degrading MB with different concentration (10, 20, 30 and 40 mg/L). The degradation rate was reduced with the increased concentration of MB solution for CdS/Ag/LPTNSs. In case of relatively dilute MB (10 mg/L), 84% degradation of MB was removed in 90 min. However, the degradation rate is decreased to 79% for 20 mg/L MB, and further declined to 50% for 40 mg/L MB. The corresponding rate constants by fitting the pseudo-first-order model can be seen in Fig. 7(d). The rate constants for degrading 10, 20, 30 and 40 mg/L for MB was 0.02, 0.017, 0.011 and 0.008 min^{-1} , respectively. Increasing the concentration of MB solution leads to more difficulty in photodegradation. The decline in photodegradation performance with increasing MB concentration can also be due to an increase in absorbed MB molecules on photocatalyst surface, which will prevent photons from reaching the photocatalyst surface, resulting in decreased photodegradation efficiency^[5].

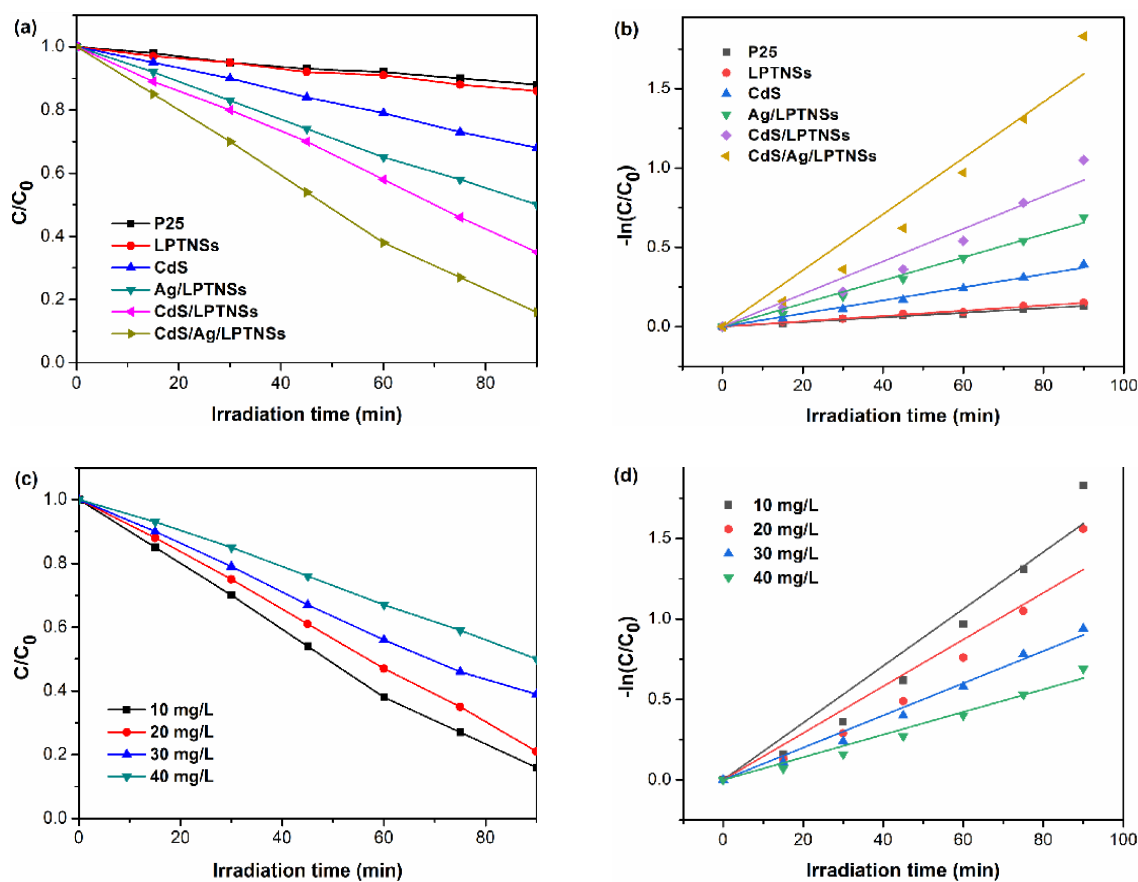


Fig. 7. (a) Photodegradation of MB with different photocatalysts and (b) corresponding pseudo-first-order kinetic fitting curves; (c) photodegradation of MB with different concentrations over CdS/Ag/TNSs and (d) corresponding pseudo-first-order kinetic fitting curves.

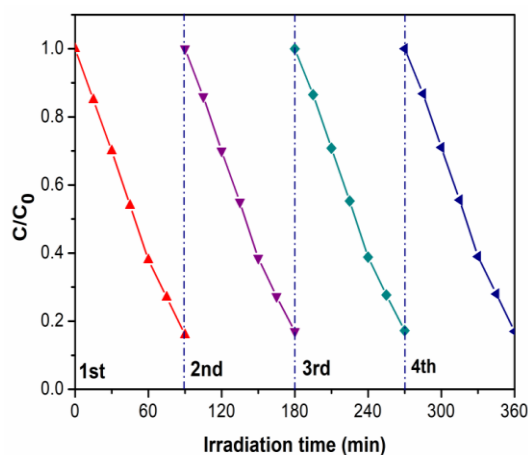


Fig. 8. Stability test of CdS/Ag/LPTNSs.

Durability is one of the significant performances for photocatalyst, therefore the repeated photocatalytic degradation performance of CdS/Ag/LPTNSs was shown in Fig. 8. Under the

identical reaction conditions, the CdS/Ag/LPTNSs was recycled for 4 times. The results show that the photocatalytic performance of CdS/Ag/LPTNSs was relatively stable. The photodegradation rate of CdS/Ag/LPTNSs towards MB still exceeds 83% after 4 cycles with slight decrease compared to the first circulation (84%).

Radical quenching experiments were used to observe the reactive species in the photocatalytic reaction. Benzoquinone (BZQ), ammonium oxalate (AO) and Tert-butanol (t-BuOH) were used as scavengers to trap $\cdot\text{O}_2^-$, h^+ and $\cdot\text{OH}$, respectively. As shown in Fig. 9, 10 mg/L of MB photodegradation rate by CdS/Ag/LPTNSs without any scavenger is about 84%. When adding t-BuOH, the degradation rate is decreased to 63%, indicating that $\cdot\text{OH}$ has a vital role in the degradation process. By using BZQ as scavenger, the rate is decreased to 22%, which shows the leading role of $\cdot\text{O}_2^-$ in the MB photodegradation. With the presence of AO, the MB degradation rate is almost unchanged.

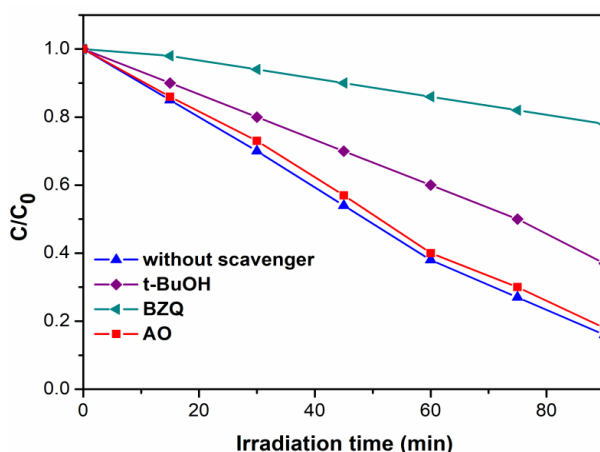


Fig. 9. Effect of reactive species scavengers on photodegradation of MB using CdS/Ag/LPTNSs.

To further distinguish the dominated reactive oxygen species during photocatalysis, ESR experiment with DMPO of the CdS/Ag/LPTNSs sample was conducted. Fig. 10 shows the obtained ESR spectra. Before light irradiation, no ESR signals of $\cdot\text{O}_2^-$ and $\cdot\text{OH}$ emitted from CdS/Ag/LPTNSs, while that of DMPO- $\cdot\text{O}_2^-$ was clearly detected after light irradiation, suggesting the formation of $\cdot\text{O}_2^-$ in the presence of CdS/Ag/LPTNSs during light irradiation. Simultaneously, the characteristic ESR signal peaks corresponding to DMPO- $\cdot\text{OH}$ also occurred during the light irradiation on CdS/Ag/LPTNSs, while the relatively low peak intensity also vetoed its controlling action in this case. In conclusion, both $\cdot\text{O}_2^-$ and $\cdot\text{OH}$ play roles in the photodegradation process, and the former is dominant reactive species.

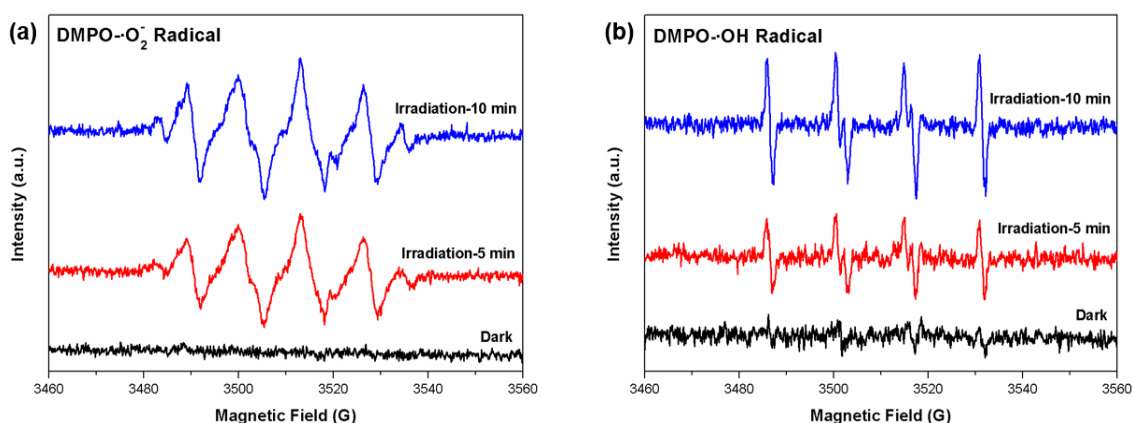


Fig. 10. ESR spectra of CdS/Ag/LPTNSs with and without light irradiation: (a) DMPO- $\cdot\text{O}_2^-$; (b) DMPO- $\cdot\text{OH}$.

3.4. Proposed photocatalytic mechanism

Based on the above analysis, the possible photodegradation mechanism for CdS/Ag/LPTNSs is shown in Fig. 11. The Ag NPs existing between CdS and LPTNSs can enhance electron transfer because of an electron relay role, facilitating the efficient separation of the generated electrons and holes. The electrons generated in the CdS by visible light excitation transfer into the conduction band of the LPTNSs through the Ag NPs, while the photogenerated holes are left in VB of CdS. The excited electron can convert O_2 into $\cdot\text{O}_2^-$, and the hole left in the VB of CdS can convert H_2O into $\cdot\text{OH}$. Finally, both $\cdot\text{O}_2^-$ and $\cdot\text{OH}$ can convert MB into CO_2 , H_2O and other small molecules. The reaction process is described as follows:

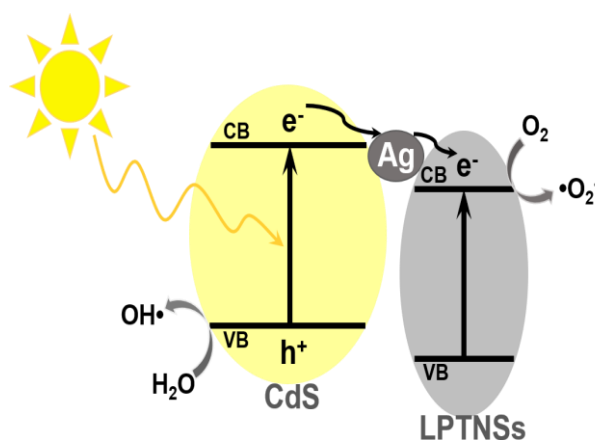
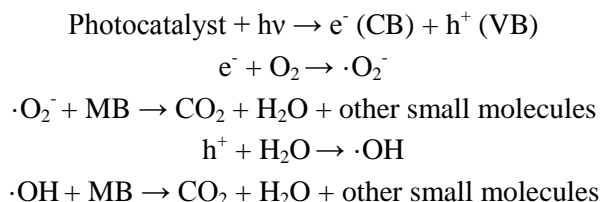


Fig. 11. Proposed photodegradation mechanism of CdS/Ag/LPTNSs.

4. Conclusion

In summary, the photocatalyst CdS/Ag/LPTNSs was successfully prepared by a two-step method. The LPTNSs sample had lamellar multilayer structure with uniformly distributed Ag and CdS particles on its surface, which is confirmed by TEM. The photodegradation rate of CdS/Ag/LPTNSs towards MB is 84% under visible light within 90 min, which is higher than that of P25, LPTNSs, CdS, Ag/LPTNSs, CdS/LPTNSs and CdS/Ag/LPTNSs. The CdS/Ag/LPTNSs displayed the better photocatalytic activity and stability due to effective separation of photogenerated electron verified by PEC and PL spectroscopy. The reactive radicals responsible for the photodegradation were identified as $\cdot\text{O}_2^-$ and $\cdot\text{OH}$. The photocatalytic mechanism has been also proposed according to the photocatalytic experiment results. Finally, the photocatalysis can remove methylene blue wastewater with high concentration, which provides a new idea for the treatment of high chroma wastewater.

Acknowledgements

This work was supported by the Basic Public Research Project of Zhejiang Province (No. LGC20B050014 and LGG18B060002), Jiaying Public Welfare Projects (No. 2020AD10021) and Scientific Training Program for College Students of Jiaying University (No. CD8517211140).

References

- [1] Z. Xu, J. Liu, K. Wang, B. Yan, S. Hu, X. Ren, Z. Gao, *Environ. Sci. Pollut. R.* 28(6), 19878 (2021); <https://doi.org/10.1007/s11356-020-11880-z>
- [1] H. Tong, S. Ouyang, Y. Bi, N. Umezawa, M. Oshikiri, J. Ye, *Adv. Mater.* 24(2), 229 (2012); <https://doi.org/10.1002/adma.201102752>
- [2] J.F. Chen, C. Hu, Z. Deng, X.P. Gong, Y. Su, Q. Yang, J.B. Zhong, J.Z. Li, R. Duan, *Chem. Phys. Lett.* 716, 134 (2019); <https://doi.org/10.1016/j.cplett.2018.12.026>
- [3] J. Ning, J. Zhang, R. Dai, Q. Wu, L. Zhang, W. Zhang, J. Yan, F. Zhang, *Appl. Surf. Sci.* 579, 152219 (2022); <https://doi.org/10.1016/j.apsusc.2021.152219>
- [4] J. Liu, S. Guo, H. Wu, X. Zhang, J. Li, K. Zhou, *J. Mater. Sci. Technol.* 85, 1 (2021).
- [5] A. Abbas, K. Li, X. Guo, A. Wu, F. Al, S. Attique, A. ul Ahmad, *Environ. Res.* 205, 112539 (2021); <https://doi.org/10.1016/j.envres.2021.112539>
- [6] M.J. Chang, W.N. Cui, J. Liu, K. Wang, H.L. Du, L. Qiu, S.M. Fan, Z.M. Luo, *J. Mater. Sci. Technol.* 36, 97 (2020); <https://doi.org/10.1016/j.jmst.2019.06.020>
- [7] I. Ali, M. Suhail, Z.A. Allothman, A. Alwarthan, *RSC Adv.* 8, 30125 (2018); <https://doi.org/10.1039/C8RA06517A>
- [8] Y. Sun, L. Chen, Y. Bao, Y. Zhang, J. Wang, M. Fu, J. Wu, D. Ye, *Catalyst* 6(12), 188 (2016); <https://doi.org/10.3390/catal6120188>
- [9] H.H. Luc, D.P. Nguyen, H. Peng, X.B. Chen, *J. Alloy. Compd.*, 744, 228 (2018); <https://doi.org/10.1016/j.jallcom.2018.02.094>

- [10] S.T. Manikkoth, K.M. Thulasi, S. Palantavida, B.K. Vijayan, *Mater. Today: Proc.* 41, 660 (2021); <https://doi.org/10.1016/j.matpr.2020.05.374>
- [11] C. Li, D. Lu, H. Wang, A. A'Lester, P. Fang, *J. Nanosci. Techno.* 19(5), 95 (2019).
- [12] M.W. Xiao, L.S. Wang, Y.D. Wu, X.J. Huang, Z. Dang, *Nanotechnology* 19, 015706 (2008); <https://doi.org/10.1088/0957-4484/19/01/015706>
- [13] T. Kameyama, K. Okazaki, K. Takagi, T. Torimoto, *Electrochemistry* 79, 776 (2011). <https://doi.org/10.5796/electrochemistry.79.776>
- [14] Y. Tian, J. Fu, B. Chang, F. Xi, X. Dong, *Mater. Lett.* 81, 95 (2012); <https://doi.org/10.1016/j.matlet.2012.04.091>
- [15] S.T. Manikkoth, K.M. Thulasi, S. Palantavida, B.K. Vijayan, *Mater. Today: Proc.* 41, 660 (2021); <https://doi.org/10.1016/j.matpr.2020.05.374>
- [16] M. Aliabadi, *Sep. Purif. Technol.* 174, 145 (2017); <https://doi.org/10.1016/j.seppur.2016.10.019>
- [17] Z. Liu, P. Fang, F. Liu, Y. Zhang, X. Liu, D. Lu, D. Li, S. Wang, *Appl. Surf. Sci.* 305, 459 (2014); <https://doi.org/10.1016/j.apsusc.2014.03.112>
- [18] W. Zhao, J. Liu, Z. Deng, J. Zhang, Z. Ding, Y. Fang, *Int. J. Hydrogen Energ.* 43, 18232 (2018); <https://doi.org/10.1016/j.ijhydene.2018.08.026>
- [19] B. Huang, Y. Yang, X. Chen, D. Ye, *Catal. Commun.* 11, 844 (2010); <https://doi.org/10.1016/j.catcom.2010.03.006>
- [20] Z. Liu, F. Chen, P. Fang, S. Wang, Y. Cao, F. Zheng, Y. Liu, Y. Dai, *Appl. Catal. A* 451, 120 (2013); <https://doi.org/10.1016/j.apcata.2012.11.020>
- [21] X. Lin, F. Rong, D. Fu, C. Yuan, *Powder Technol.* 219, 173 (2012); <https://doi.org/10.1016/j.powtec.2011.12.037>
- [22] P. Gao, J. Liu, D. Sun, W. Ng, *J. Hazard. Mater.* 250-251, 412 (2013); <https://doi.org/10.1016/j.jhazmat.2013.02.003>
- [23] S. Le, W. Li, Y. Li, B. Borjigin, G. Li, X. Wang, *Photochem. Photobiol.* 95, 501 (2019); <https://doi.org/10.1111/php.12992>
- [24] B. Zhai, Y. Chen, Y. Liang, *J. Nanopart. Res.* 21, 265 (2019); <https://doi.org/10.1007/s11051-019-4704-1>
- [25] X. Yuan, H. Wang, Y. Wu, G. Zeng, X. Chen, L. Leng, Z. Wu, H. Li, *Appl. Organomet. Chem.* 30, 289 (2016); <https://doi.org/10.1002/aoc.3430>
- [26] J. Ning, J. Zhang, R. Dai, Q. Wu, L. Zhang, W. Zhang, J. Yan, F. Zhang, *Appl. Surf. Sci.* 579, 152219 (2022); <https://doi.org/10.1016/j.apsusc.2021.152219>